Karl-Franzens-Universität Graz
Institut für Physik, Fachbereich Theoretische Physik

Der Wissenschaftsfonds.

Lattice quark propagator in Coulomb gauge: renormalization and confinement

G. Burgio,[1] M. Schröck,[2] H. Reinhardt,[1] M. Quandt[1]

[1]Institut für Theoretische Physik, 72076 Tübingen, Germany, [2]Institut für Physik, FB Theoretische Physik, Universität Graz, 8010 Graz, Austria.

Introduction

The main issue addressed in all lattice analysis of pure Yang–Mills theories in Coulomb gauge has been the renormalizability of Green's functions; indeed, it has been shown in e.g. Ref. [1] that for *static* correlators a non-perturbative renormalization procedure can be defined in the lattice Hamiltonian limit $a_t \to 0$.

We show that, as for the gluon, the lattice Coulomb gauge *static* quark propagator $S(\boldsymbol{p}) = \int dp_4 S(p)$ is renormalizable; from $S(\boldsymbol{p})$ the renormalization function $Z(|\boldsymbol{p}|)$ and the running mass $M(|\boldsymbol{p}|)$ can be extracted. We also find that, at least for improved actions closer to the continuum limit, the full propagator $S(p)$ has a trivial energy dependence, making it also renormalizable and allowing for a definition of the quark dispersion relation compatible with the confining properties of the theory.

Gauge field configurations

Our calculations have been performed on nine sets of gauge field configurations generated by the MILC collaboration [2, 3], made available via the Gauge Connection. The configurations were produced with the Symanzik-improved Lüscher–Weisz gauge action; seven out of nine sets include two light degenerate (u, d) and one heavier (s) quark flavor, while two are in the quenched approximation; all dynamical calculations used the Asqtad improved action.

	$L^3 \times T$	a [fm]	am	m [MeV]	# config.
(a)	$20^3 \times 64$	0.121	0.010, 0.050	15.7, 78.9	202
(b)	$20^3 \times 64$	0.121	0.020, 0.050	31.5, 78.9	50
(c)	$20^3 \times 64$	0.120	0.030, 0.050	47.3, 78.9	25
(d)	$20^3 \times 64$	0.119	0.040, 0.050	63.1, 78.9	25
(e)	$20^3 \times 64$	0.121	–	–	66
(f)	$28^3 \times 96$	0.086	0.0062, 0.031	14.0, 67.8	50
(g)	$28^3 \times 96$	0.086	0.0124, 0.031	27.1, 67.8	50
(h)	$28^3 \times 96$	0.086	–	–	77
(i)	$64^3 \times 144$	0.060	0.0036, 0.0108	11.8, 35.3	5

Quark propagator in Coulomb gauge

The tree-level continuum quark propagator reads in Euclidean space:

$$S^{(0)}(p)^{-1} = i\not{\boldsymbol{p}} + i\not{p}_4 + m\,, \tag{1}$$

where we have explicitely separated the spatial momenta p_i from the temporal one p_4 (the energy) to make contact with the non-manifestly Euclidean invariant interacting Coulomb gauge propagator $S^{-1}(p)$. The latter can be decomposed as

$$S^{-1}(p) = i\not{\boldsymbol{p}} A_s(|\boldsymbol{p}|, p_4) + i\not{p}_4 A_t(|\boldsymbol{p}|, p_4) + B_m(|\boldsymbol{p}|, p_4) \tag{2}$$

with scalar functions $A_s(|\boldsymbol{p}|, p_4)$, $A_t(|\boldsymbol{p}|, p_4)$ and $B_m(|\boldsymbol{p}|, p_4)$, to which we will refer as the spatial, temporal and massive component, respectively. We found the possible fourth component $\propto \sum_j p_j \sigma_{j4}$ to be zero [4] and thus will not further consider it here.

Renormalizability

Due to the energy independence of the dressing functions Eq. (2) [4], we can average them over p_4 to minimize statistical fluctuations. The full propagator thus reads

$$S^{-1}(p) = i\not{\boldsymbol{k}} a A_s(|\boldsymbol{p}|) + i\not{k}_4 a A_t(|\boldsymbol{p}|) + B_m(|\boldsymbol{p}|)\,, \tag{3}$$

while its static counterpart is obviously:

$$S^{-1}(\boldsymbol{p}) = i\not{\boldsymbol{k}} a A_s(|\boldsymbol{p}|) + B_m(|\boldsymbol{p}|)\,, \tag{4}$$

since Eq. (3) is even in p_4 and thus the temporal component, when integrated from $-\pi$ to π, will vanish. Here, $k = k(p)$ denotes the Asqtad lattice momentum.

We can now define from Eq. (3), Eq. (4) the static propagator

$$S_\zeta(\boldsymbol{p}) = \frac{Z_\zeta(|\boldsymbol{p}|)}{i\not{\boldsymbol{p}} + M(|\boldsymbol{p}|)}\,. \tag{5}$$

and its non-static counterpart

$$S_\zeta(p) = \frac{Z_\zeta(|\boldsymbol{p}|)}{ia\not{\boldsymbol{k}} + ia\not{k}_4 \alpha(|\boldsymbol{p}|) + M(|\boldsymbol{p}|)}\,, \tag{6}$$

where the renormalization function $Z(|\boldsymbol{p}|)$, the mass function $M(|\boldsymbol{p}|)$ and the "running energy" $\alpha(|\boldsymbol{p}|)$ are given by

$$Z(|\boldsymbol{p}|) = \left(\int_{-\pi}^{\pi} \frac{\mathrm{d}\hat{p}_4}{2\pi} A_s(|\boldsymbol{p}|, p_4)\right)^{-1}$$

$$\alpha(|\boldsymbol{p}|) = \frac{\int_{-\pi}^{\pi} \frac{\mathrm{d}\hat{p}_4}{2\pi} A_t(|\boldsymbol{p}|, p_4)}{\int_{-\pi}^{\pi} \frac{\mathrm{d}\hat{p}_4}{2\pi} A_s(|\boldsymbol{p}|, p_4)}, \qquad M(|\boldsymbol{p}|) = \frac{\int_{-\pi}^{\pi} \frac{\mathrm{d}\hat{p}_4}{2\pi} B_m(|\boldsymbol{p}|, p_4)}{\int_{-\pi}^{\pi} \frac{\mathrm{d}\hat{p}_4}{2\pi} A_s(|\boldsymbol{p}|, p_4)}. \tag{7}$$

The integrals are intended as statistical average. To check renormalizability we therefore now need to establish the scale invariance of M and, for the full propagator, of α on one side, and the scaling properties of Z on the other side.

Results

In Fig. 1a we show the mass function $M(|\boldsymbol{p}|)$ from configuration sets (a)–(d), with scale $a \approx 0.12\,\mathrm{fm}$, compared to configuration sets (f) and (g), which have a scale $a = 0.086\,\mathrm{fm}$. These sets are chosen to have approximately the same physical volume, so to minimize finite size effects at the two different cutoffs. As can be seen, $M(|\boldsymbol{p}|)$ nicely agrees for the sets with similar masses.

We compare the corresponding wave-function renormalization functions $Z(|\boldsymbol{p}|)$ from configuration sets (g) and (b) in Fig. 1b, finding a good agreement once we rescale both to $Z(\zeta) = 1$ for $\zeta = 3.0\,\mathrm{GeV}$.

We can thus conclude that the static propagator Eq. (5) is multiplicative renormalizable.

Turning now to the full propagator Eq. (6), Fig. 1c shows the function α, i.e. the ratio A_t to A_s, from different configuration sets. The scaling behaviour is very good and we can thus conclude that the full propagator Eq. (6) is also multiplicative renormalizable; this allows us to define a dispersion relation for the quark as in Eq. (8).

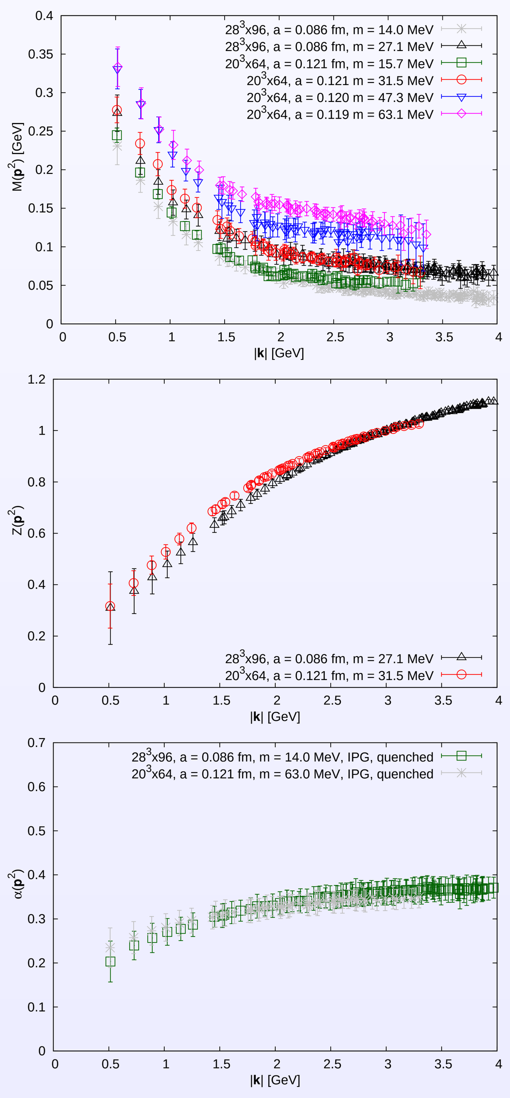

Figure 1: Top to bottom: $M(|\boldsymbol{p}|)$ from sets (a)-(g), $Z(|\boldsymbol{p}|)$ from sets (f) and (i), $\alpha(|\boldsymbol{p}|)$ from sets (e), (h).

Confinement

From the full non-static propagator Eq. (6) we can directly read from the resolution of its poles in p_4, or equivalently intergration in p_4, the effective energy:

$$E(|\boldsymbol{p}|) = \frac{1}{\alpha(|\boldsymbol{p}|)}\sqrt{\boldsymbol{p}^2 + M^2(|\boldsymbol{p}|)}\,. \tag{8}$$

Interestingly, α in Fig. 1c tends to be suppressed in the IR, enhancing E. If α should indeed prove to vanish in the IR, $\alpha(|\boldsymbol{p}|) \propto |\boldsymbol{p}|^k$, we would have for the quark dispersion relation a behaviour qualitatively similar to the Gribov formula for the gluon [5, 1], explaning quark confinement with an IR diverging effective energy, $E \propto |\boldsymbol{p}|^{-k}$.

Comparison to Landau gauge

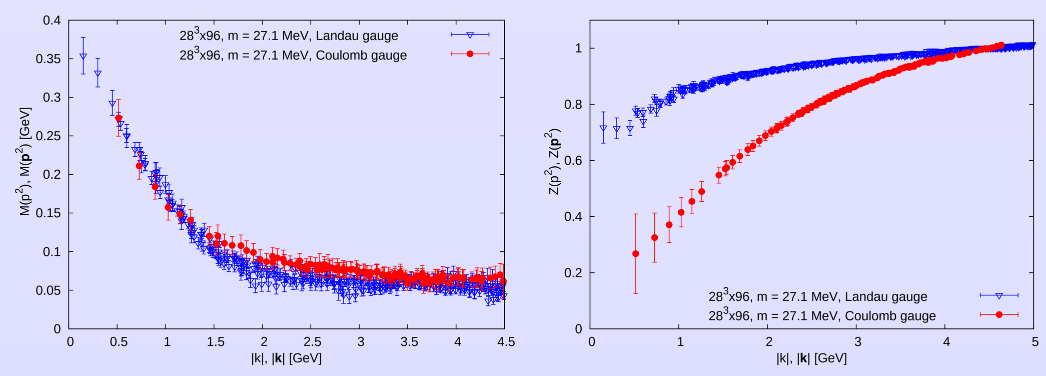

Figure 2: Landau vs. Coulomb gauge: $M(|\boldsymbol{p}|)$ (left) and $Z(|\boldsymbol{p}|)$ (right) from (f).

In Fig. 2 we show the comparison between the mass and renormalization functions in Coulomb and Landau gauge, the latter taken from Ref. [6]. Apart for a slight difference in the intermediate momentum region M almost coincides in both gauges, while as expected Z, where the renormalization point ζ has been set at the largest available momentum in Coulomb gauge, 4.64 GeV, shows a much stronger gauge dependence.

Chiral limit

In Fig. 3a we have attempted for the configurations (a)–(d), where the dynamical masses diminish at constant cutoff, a chiral extrapolation of the mass function determined for Asqtad fermions at the dynamical point, so to avoid systematic errors due to partial quenching. In Fig. 3b we show the chiral extrapolation for configuration (i) with Kogut-Susskind fermions, where the mass has been fixed to five different values, with only the last at the dynamical point. Within error bars the two extrapolations agree.

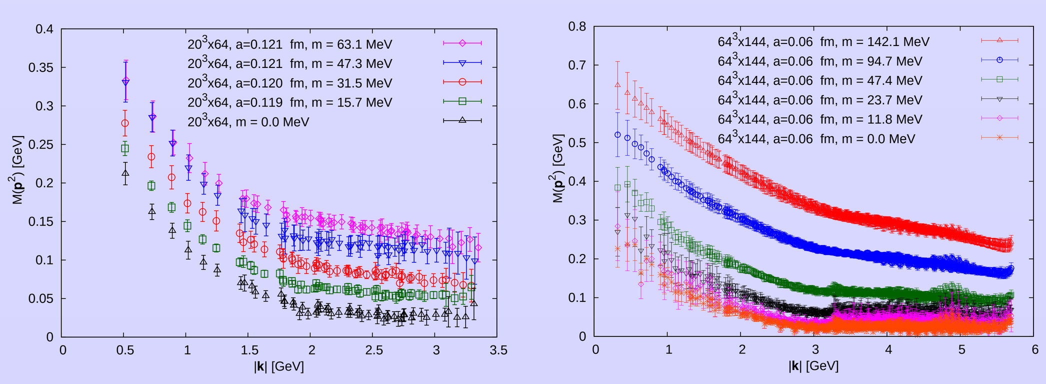

Figure 3: Chiral limits: M from (a)–(d) (left) and from (i) (right).

References

[1] G. Burgio, M. Quandt, and H. Reinhardt, Phys. Rev. Lett. **102**, 032002 (2009), 0807.3291.

[2] C. W. Bernard *et al.*, Phys.Rev. **D64**, 054506 (2001), hep-lat/0104002.

[3] C. Aubin *et al.*, Phys.Rev. **D70**, 094505 (2004), hep-lat/0402030.

[4] G. Burgio, M. Schröck, H. Reinhardt, and M. Quandt, in preparation (2012).

[5] V. N. Gribov, Nucl. Phys. **B139**, 1 (1978).

[6] P. O. Bowman *et al.*, Phys.Rev. **D71**, 054507 (2005), hep-lat/0501019.